

Pulse-gated mode of commercial superconducting nanowire single photon detectors

Fan Liu(刘帆), Mu-Sheng Jiang(江木生), Yi-Fei Lu(陆宜飞), Yang Wang(汪洋), and Wan-Su Bao(鲍皖苏)
Citation: Chin. Phys. B, 2021, 30 (**4**): 040302. DOI: 10.1088/1674-1056/abc2c2
Journal homepage: http://cpb.iphy.ac.cn; http://iopscience.iop.org/cpb

What follows is a list of articles you may be interested in

Deterministic nondestructive state analysis for polarization-spatial-time-bin hyperentanglement with cross-Kerr nonlinearity

Hui-Rong Zhang(张辉荣), Peng Wang(王鹏), Chang-Qi Yu(于长琦), and Bao-Cang Ren(任宝藏)
Chin. Phys. B, 2021, 30 (**3**): 030304. DOI: 10.1088/1674-1056/abd7d5

One-decoy state reference-frame-independent quantum key distribution

Xiang Li(李想), Hua-Wei Yuan(远华伟), Chun-Mei Zhang(张春梅), Qin Wang(王琴)
Chin. Phys. B, 2020, 29 (**7**): 070303. DOI: 10.1088/1674-1056/ab90f6

Detection efficiency characteristics of free-running InGaAs/InP single photon detector using passive quenching active reset IC

Fu Zheng(郑福), Chao Wang(王超), Zhi-Bin Sun(孙志斌), Guang-Jie Zhai(翟光杰)
Chin. Phys. B, 2016, 25 (**1**): 010306. DOI: 10.1088/1674-1056/25/1/010306

Statistical analysis of the temporal single-photon response of superconducting nanowire single photon detection

He Yu-Hao, Lü Chao-Lin, Zhang Wei-Jun, Zhang Lu, Wu Jun-Jie, Chen Si-Jing, You Li-Xing, Wang Zhen
Chin. Phys. B, 2015, 24 (**6**): 060303. DOI: 10.1088/1674-1056/24/6/060303

Performance of superconducting nanowire single-photon detector with the fan coupling antenna array

Wang Yu-Jue, Ding Tian, Ma Hai-Qiang, Jiao Rong-Zhen
Chin. Phys. B, 2014, 23 (**6**): 060308. DOI: 10.1088/1674-1056/23/6/060308

Pulse-gated mode of commercial superconducting nanowire single photon detectors*

Fan Liu(刘帆)[1,2], Mu-Sheng Jiang(江木生)[1,2,†], Yi-Fei Lu(陆宜飞)[1,2], Yang Wang(汪洋)[1,2], and Wan-Su Bao(鲍皖苏)[1,2]

[1] *Henan Key Laboratory of Quantum Information and Cryptography, SSF IEU, Zhengzhou* 450001, *China*

[2] *Synergetic Innovation Centre of Quantum Information and Quantum Physics, University of Science and Technology of China, Hefei* 230026, *China*

(Received 8 August 2020; revised manuscript received 15 September 2020; accepted manuscript online 20 October 2020)

High detection efficiency and low intrinsic dark count rate are two advantages of superconducting nanowire single photon detectors (SNSPDs). However, the stray photons penetrated into the fiber would cause the extrinsic dark count rate, owing to the free running mode of SNSPDs. In order to improve the performance of SNSPDs in realistic scenarios, stray photons should be investigated and suppression methods should be adopted. In this study, we demonstrate the pulse-gated mode, with 500 kHz gating frequency, of a commercial SNSPD system for suppressing the response of stray photons about three orders of magnitude than its free-running counterpart on the extreme test conditions. When we push the gating frequency to 8 MHz, the dark count rate still keeps under 4% of free-running mode. In experiments, the intrinsic dark count rate is also suppressed to 4.56×10^{-2} counts per second with system detection efficiency of 76.4372%. Furthermore, the time-correlated single-photon counting analysis also approves the validity of our mode in suppressing the responses of stray photons.

Keywords: quantum detector, superconducting nanowire, pulse gated, dark count rate

PACS: 03.67.Dd, 03.67.Hk, 03.67.–a **DOI:** 10.1088/1674-1056/abc2c2

1. Introduction

Superconducting nanowire single-photon detectors (SNSPDs) have rapidly emerged as highly promising photon-counting technology in various experiments and applications (e.g., quantum key distribution, quantum optical and biological applications) with high system detection efficiency (SDE), low intrinsic dark count rate (DCR) and small timing jitter.[1–7]

Since SDE and DCR both correlate with bias current, the figure of merit of SNSPDs correlates is often represented as the SDE at a specific DCR.[2,4] In the last decade, much effort has been devoted to improve SDE in structure and material innovation, whereas suppressing DCR attracted relatively little attention.[8–13] As a matter of fact, detecting very faint signals requires not only high SDE, but also very low DCR. For example, in long-distance quantum key distribution (QKD) experiments, the quantum bit error rate (QBER), limiting the secure transmission distance, is dominated by the DCR of the detectors. The SDE of SNSPD, used in the QKD distance of 260 km, only reached 3%, owing to suppression of DCR from reducing bias current.[14] Therefore, suppressing of DCR plays an essential role as well as that of increasing SDE in practical applications.

The DCR includes two regions, i.e., intrinsic DCR (iDCR) and extrinsic DCR (eDCR). The iDCR, accounting for the primary role of high bias current region, correlates to the spontaneous vortex motion on the nanowire.[15] Meanwhile, the eDCR, dominating the region of low bias current, associates with the noise photons from both the blackbody radiation of the fiber itself and stray photons penetrated into the fiber.[12,13]

Researchers have indicated that lowering SNSPDs base temperature could reduce the iDCR and lower target temperature leads to smaller eDCR.[16,17] Shibata *et al.* effectively improved the DCR by 29 dB with 2.4 dB decreasing of the SDE using various cold filters.[12,13] Meanwhile, Yang *et al.* suppressed the eDCR by two orders of magnitude via applying an on-chip band-pass filter to SNSPD devices.[11] However, these techniques, namely coupling filter on SNSPD devices, will be elusive for common investigators. Moreover, additional optical components increase cost and reduce reliability, e.g., the SDE will decrease in most circumstances.

There is familiar problem in avalanche photodiodes (APDs) with a high dark count probability caused by the thermal effect due to high bias current. The gate-mode quenching technique is applied to deal with it.[18] Also, the sine-gated mode (SGM) has been used in a home-made SNSPD system by Akhlaghi, to improve the maximal count rate.[19] In this paper, we apply a pulse bias current on the nanowire to actively quench the response stray photons and the intrinsic dark count rate. In our experiments, a commercial SNSPD in this operation, denoted as pulse-gated mode (PGM) with 500 kHz gating frequency, can suppress the DCR to 4.56×10^{-2} counts

*Project supported by the National Natural Science Foundation of China (Grant No. 61605248) and the National Basic Research Program of China (Grant No. 2013CB338002).

†Corresponding author. E-mail: jmusheng@139.com

© 2021 Chinese Physical Society and IOP Publishing Ltd

per second with SDE of 76.4372%.

2. Description of commercial SNSPDs

The commercial SNSPD devices used in this work are fabricated by PHOTEC, Shanghai, China.[20] The schematic diagram of this system is shown in Fig. 1(a). Most commercial SNSPDs are thus far operated in free-running mode (FM), namely, a constant current I_b, only slightly smaller than critical current, is applied on the nanowires.[21] Therefore, even the energy carried by a single photon can lead to formation of a hot resistive bridge across the width of nanowires resulting a rising voltage, as shown in Fig. 1(b), as a photon detection signal.

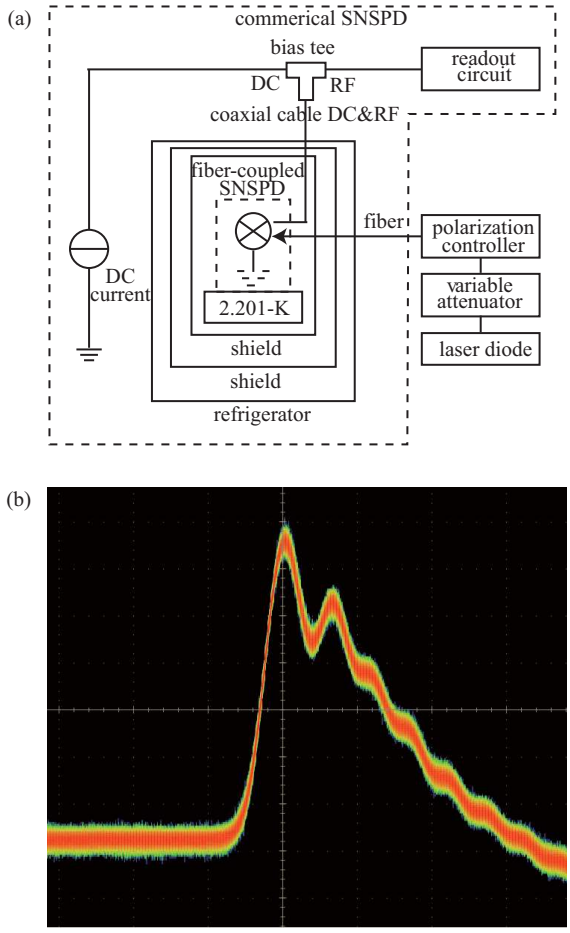


Fig. 1. The free-running mode operation of superconducting nanowire single photon detectors (SNSPDs). (a) Schematic of the commercial SNSPD under free-running mode in which the nanowire under test is cooled to 2.201 K by a cryocooler. (b) Waveforms for dark event recorded by an oscilloscope with width of 80 ns.

To gauge the SDE and DCR at a given I_b, a photon counter is often adopted to count the response pulse with amplitude larger than a specific threshold. According to the definition widely used, the response pulse count rate, when the input fiber to the cryocooler is blocked, is defined as the iDCR. For measuring the SDE, we should illuminate the SNSPD with a given photon flux using pulsed or continuous-wave (CW) light sources.[17,22] However, the eDCR plays a more essential role than iDCR when the SNSPD is illuminated. Therefore, in the paper, we measure the DCR (sum of iDCR and eDCR) by blocking the illumination from the light source.

To show the influence of eDCR, we measure the SDE and DCR of two channels of FM-SNSPD on different times of days. The measurements are obtained in a room with windows but without direct sunlight, except iDCR which is determined in a dark room. We use a pulsed laser with a typical pulse width of 50 ps and various pulse repetition rates (R_{re}). In our experiment, R_{re} is set to 500 kHz, thus the number of 5×10^4 photons per second corresponds to an averaged 0.1 photons per pulse.

Figures 2(a) and 2(b) show the SDE and DCR, as functions of I_b, for the channel 1 of FM-SNSPD on different times of days. The SDE and DCR for the channel 2 of FM-SNSPD are displayed in Figs. 2(c) and 2(d). The SDEs for one channel of FM-SNSPD in various measurements are only slightly different, meanwhile, the DCR have great differences under variety of scenarios and significantly outnumber the intrinsic dark count rate. We attribute the fluctuation of DCR to the change of stray photons penetrated into the fiber, which depend on the illumination from outside. The results manifest that the stray photons, from both the blackbody radiation of the fiber and the stray light penetrated into the fiber, dominate the DCR in the practical applications.

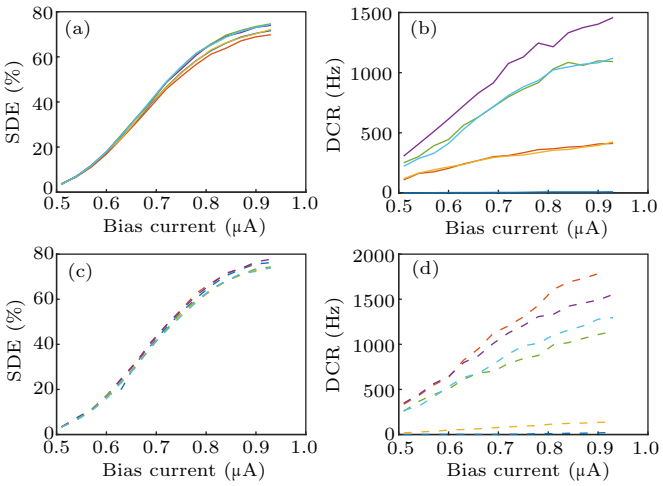


Fig. 2. The system detection efficiency (SDE) and dark count rate (DCR) for two channels of FM-SNSPD on different times of days. The solid lines are the results about channel 1 of FM-SNSPD, and the dashed lines are the results about channel 2 of FM-SNSPD. These measurements are taken on different times of days, and the weathers in those days were different.

3. The principle of PGM-SNSPD

We use the schematic shown in Fig. 3(a) to implement a PGM-SNSPD. A commercial SNSPD is biased by a pulse current, combined with a DC current via a T-junction at the DC&RF port of the bias-tee. There is a low-pass filter, to extract signals from noise, placed between the readout circuit and the RF port of the bias-tee. The output signals are converted to LVTTL signals by the amplifying and shaping circuit.

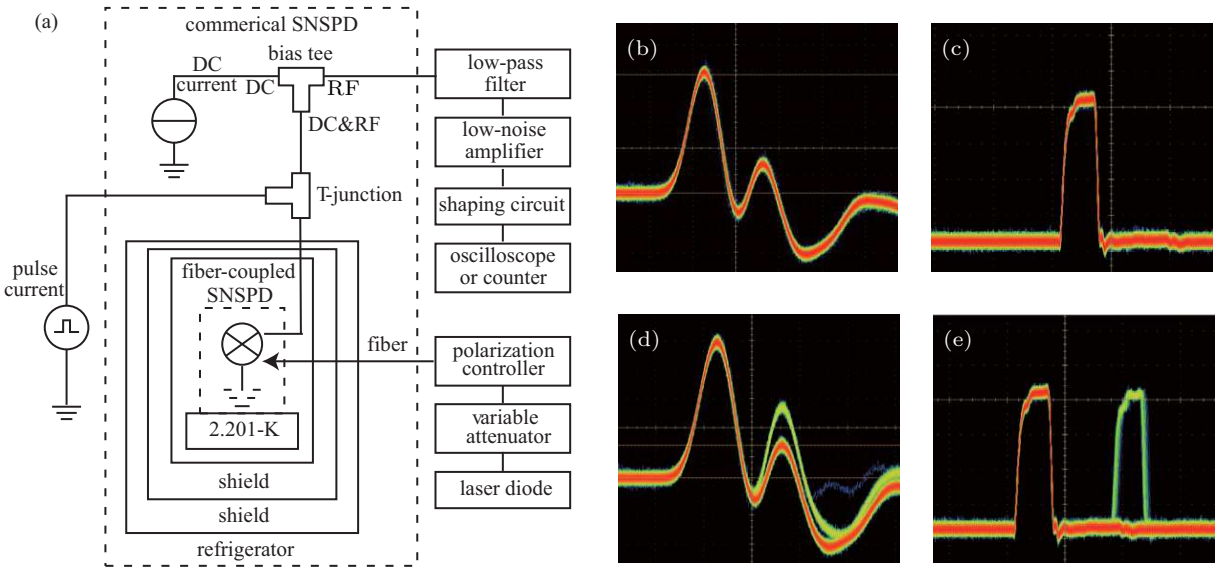


Fig. 3. The pulse-gated mode (PGM) operation of SNSPDs. (a) Schematic of the PGM-SNSPD in which the nanowire under test is cooled to 2.201 K by a cryocooler. (b) Waveforms for gating pulse recorded by an oscilloscope before shaping. (c) Waveforms for gating pulse recorded by an oscilloscope after shaping. (d) Waveforms recorded by an oscilloscope when there are response signals of photons before shaping. (e) Waveforms recorded by an oscilloscope when there are response signals of photons after shaping. Note that the first red signal is idle pulse, which will be subtracted in practical applications, we do not deal with it in proof-of-principle experiments. The photon detection signals are the green pulses in (d) and (e).

Figure 3(b) is the signals without photon responses before shaping, with two main peaks. The former is an idle pulse divided at the T-junction and should be subtracted due to no effect on photons responses. This pulse cannot be eliminated completely by filters, owing to the broad spectrum of pulse. Figure 3(c) shows the signals caused by the idle pulses in Fig. 3(b), after the reshaping circuits. Fortunately, the arrival time of idle pulses maintain in a region, which can be easily distinguished in the time. Actually, replacing the T-junction with a broad spectrum circulator can avoid this idle pulse. Hence, we roughly dismiss the idle pulse in the photon counting. The latter pulse in Fig. 3(b) is the reflection of the efficient pulse superimposed on the nanowire, owing to the impedance mismatches at junction of coaxial cable and nanowire. By adjusting time delay, the pulsed laser can be locked to the peak of the pulse current through SNSPD. Figure 3(c) has tow parts of signal without and with photon detected signals, marked as red and green, respectively. In the shaping circuit, accurate threshold setting can filter out pulse gate, without signal, and signal response in other time slots. As shown in Fig. 3(e), the first red signal is the idle pulse and the second green signal is the photon detection response.

4. Concept and model

First of all, we quantitatively compare the DCR of the three operating modes. Figure 4 shows the cyclical current on the nanowires under three different modes of SNSPD. In the FM, the bias current is a constant DC current, denoted as $I_{\mathrm{B,FM}}$. In the SGM, the bias current takes the form[19]

$$I_{\mathrm{B,SGM}}(t) = I_{\mathrm{Dc,SGM}} + I_{\mathrm{Ch,SGM}}(t), \tag{1}$$

where the $I_{\mathrm{Dc,SGM}}$ is constant current and

$$I_{\mathrm{Ch,SGM}}(t) = A_{\mathrm{SGM}} \sin(2\pi T t), \tag{2}$$

t labels the time and T is the cycle.

In the PGM, the bias current takes the form

$$I_{\mathrm{B,PGM}}(t) = I_{\mathrm{DC,PGM}} + I_{\mathrm{Ch,PGM}}(t), \tag{3}$$

where $I_{\mathrm{Dc,PGM}}$ and $I_{\mathrm{Ch,PGM}}(t) = \tau A_{\mathrm{PGM}}$ $\{$if $t_1 \le t \le t_2$, $\tau = 1$ else $\tau = 0\}$ are the DC and AC components of the bias, t_1 and t_2 label the pulse rising and falling edges.

According to the FM-SNSPD measurement in Figs. 2(c) and 2(d), we fitted the SDE and DCR as functions of the bias current, and assumed that the dark count rate in the dark room is the iDCR of channel 2 of SNSPD.

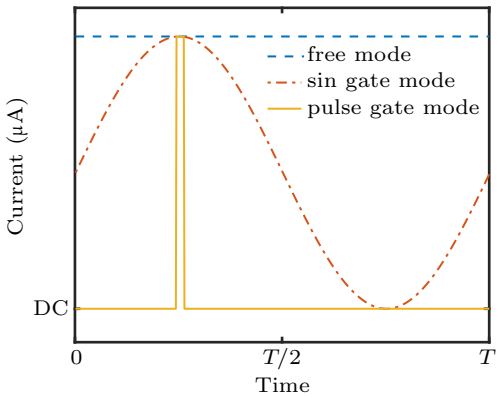


Fig. 4. The current on the nanowire under three different modes of SNSPDs as the function of the time in which the dashed line is a constant function and the chain line and solid line are simulated based on Eqs. (1) and (2), respectively.

For PGM and SGM gate between $0 \le t < T$, the iDCR between t and $t + \Delta t$ equals to $\mathrm{iDCR_{FM}} I_{\mathrm{B}}(t)\Delta t$,[19] and eDCR

can be defined as

$$\mathrm{eDCR}\left(I_{\mathrm{B}}\left(t\right)\right)=\mathrm{SDE}\left(I_{\mathrm{B}}\left(t\right)\right)N_{\mathrm{stray}}\Delta t, \tag{4}$$

provided that the detector has not already been latched in the same gate. We can define the DCR of the FM, PGM and SGM in Δt as

$$\begin{aligned}&\mathrm{DCR}_{\mathrm{FM}}(t)\,\mathrm{d}t\\ =\;&\left[\mathrm{iDCR}_{\mathrm{FM}}(I_{\mathrm{B,FM}}(t))+\mathrm{SDE}_{\mathrm{FM}}(I_{\mathrm{B,FM}}(t))\right]\mathrm{d}t\\ &\times\left[1-\int_0^t\mathrm{DCR}_{\mathrm{FM}}(t)\,\mathrm{d}t\right],\end{aligned} \tag{5}$$

$$\begin{aligned}&\mathrm{DCR}_{\mathrm{PGM}}(t)\,\mathrm{d}t\\ =\;&\left[\mathrm{iDCR}_{\mathrm{PGM}}(I_{\mathrm{B,PGM}}(t))+\mathrm{SDE}_{\mathrm{PGM}}(I_{\mathrm{B,PGM}}(t))\right]\mathrm{d}t\\ &\times\left[1-\int_0^t\mathrm{DCR}_{\mathrm{PGM}}(t)\,\mathrm{d}t\right],\end{aligned} \tag{6}$$

$$\begin{aligned}&\mathrm{DCR}_{\mathrm{SGM}}(t)\,\mathrm{d}t\\ =\;&\left[\mathrm{iDCR}_{\mathrm{SGM}}(I_{\mathrm{B,SGM}}(t))+\mathrm{SDE}_{\mathrm{SGM}}(I_{\mathrm{B,SGM}}(t))\right]\mathrm{d}t\\ &\times\left[1-\int_0^t\mathrm{DCR}_{\mathrm{SGM}}(t)\,\mathrm{d}t\right].\end{aligned} \tag{7}$$

Thence, the average of DCR in the FM, PGM and SGM in a period would be

$$\begin{aligned}\overline{\mathrm{DCR}_{\mathrm{FM}}}&=\frac{1}{T}\int_0^T\mathrm{DCR}_{\mathrm{FM}}(t)\,\mathrm{d}t\\ &=\frac{1}{T}\left[1-\exp\left(-\int_0^T\left(\mathrm{iDCE}_{\mathrm{FM}}(I_{\mathrm{B,FM}})\right.\right.\right.\\ &\quad\left.\left.\left.+\mathrm{SDE}_{\mathrm{FM}}(I_{\mathrm{B,FM}}(t))\right)\mathrm{d}t\right)\right],\end{aligned} \tag{8}$$

$$\begin{aligned}\overline{\mathrm{DCR}_{\mathrm{PGM}}}&=\frac{1}{T}\int_0^T\mathrm{DCR}_{\mathrm{PGM}}(t)\,\mathrm{d}t\\ &=\frac{1}{T}\left[1-\exp\left(-\int_0^T\left(\mathrm{iDCE}_{\mathrm{PGM}}(I_{\mathrm{B,PGM}})\right.\right.\right.\\ &\quad\left.\left.\left.+\mathrm{SDE}_{\mathrm{PGM}}(I_{\mathrm{B,PGM}}(t))\right)\mathrm{d}t\right)\right],\end{aligned} \tag{9}$$

$$\begin{aligned}\overline{\mathrm{DCR}_{\mathrm{SGM}}}&=\frac{1}{T}\int_0^T\mathrm{DCR}_{\mathrm{SGM}}(t)\,\mathrm{d}t\\ &=\frac{1}{T}\left[1-\exp\left(-\int_0^T\left(\mathrm{iDCE}_{\mathrm{SGM}}(I_{\mathrm{B,SGM}})\right.\right.\right.\\ &\quad\left.\left.\left.+\mathrm{SDE}_{\mathrm{SGM}}(I_{\mathrm{B,SGM}}(t))\right)\mathrm{d}t\right)\right].\end{aligned} \tag{10}$$

We use the function fitted from Fig. 2 and parameters in Table 1 to simulate the dark count in three modes, with different amounts of stray photons. The results are shown in Fig. 5. The number of stray photons are 50, 5×10^2, 5×10^3 and 5×10^4 photons per second in Figs. 5(a)–5(d), respectively. It is shown that even with extremely large numbers of stray photons, PGM-SNSPDs can still maintain extremely low dark counts. In fact, the dark count rate in our PGM is about three orders of magnitude smaller than the corresponding dark count rate in FM and SGM.

Table 1. Simulation parameters.

Variable	Parameter	Simulation value
$I_{\mathrm{B,FM}}$	current for FM-SNSPD	$I_{\mathrm{DC}}+0.48$
$I_{\mathrm{B,SGM}}$	current for SGM-SNSPD	$I_{\mathrm{DC}}+0.48(1+\sin(2T\pi t))$
$I_{\mathrm{B,PGM}}$	current for PGM-SNSPD	$I_{\mathrm{DC}}+0.48\tau$, $t_2-t_1=8$ ns
R_{re}	pulse repetition rates	500 kHz
N_{stray}	number of stray photons per second	50, 5×10^2, 5×10^3, 5×10^4

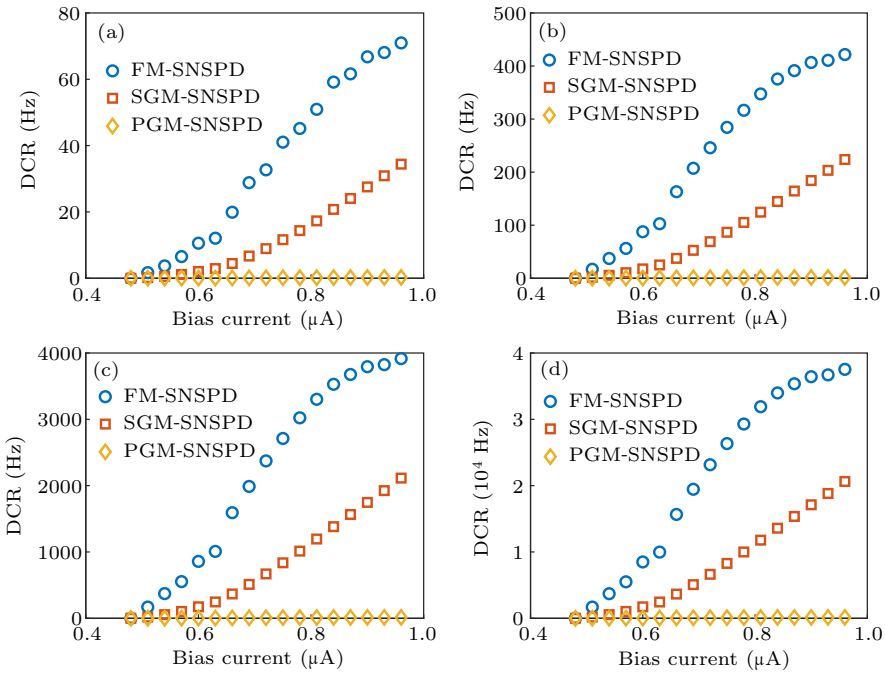


Fig. 5. The simulation of dark count rate in three modes with different numbers of stray photons in which circles are simulated based on Eq. (6), the squares are simulated based on Eq. (7) and the diamonds are simulated based on Eq. (8). Here we use the functions of system detection efficiency and dark count rate fitted by the data measured in Figs. 2(c) and 2(d) and the number of stray photons are set as 50, 5×10^2, 5×10^3 and 5×10^4 photons per second, respectively.

5. Experimental characterization

We excite the detectors using a 1550 nm pulse laser, through a variable attenuator, at a level that makes the measured count rates linearly proportional to the laser intensity, thus ensuring single photon sensitivity. The width of bias pulse is 8 ns and the frequency of bias pulse is 500 K. We measure the SDE and DCR for two channels of PGM-SNSPDs. Remarkably, by adjusting the threshold, we could suppress the DCRs of two channels to sub-Hz, which are hard to measure accurately in a short time. Therefore, we do not show the DCR in Fig. 6(a). Since natural light is constantly changing, it is difficult to perform long-term measurements under the same conditions. To more accurately demonstrate the suppression of dark counts caused by stray photons by PGM, we use a 1550 nm continuous wave (CW) laser to simulate stray photons in the fiber. In Figs. 6(b)–6(d), we inject a certain intensity of stray photons to make the maximum DCR in FM-SNSPD about 2000, which is a mid condition in practical conditions. Figure 6(b) shows the results of FM-SNSPD. It can be observed that the growth trend of DCR is basically the same as that of SDE. Figure 6(c) is the SDE and DCR for PGM-SNSPD with 500 kHz pulse frequency. The DCR is suppressed by about 3 orders of magnitude with a basically unchanged SDE.

In Fig. 6(d), we try to increase the pulse frequency of PGM-SNSPD. However, due to the performance limitation of our pulse generator, we can only get a pulse with full width half maximum of 8 ns. The overshoot of amplifier causes the signal width to reach about 150 ns. Therefore, we set the repetition frequency of the gating pulse to 8 MHz. As shown in Fig. 6(d), the SDE can still be maintained with high level and the DCR is about 4% of Fig. 6(b).

To show the influence of different operation mode on extreme test conditions, we measure the DE and DCR of FM-SNSPD, 500k-PGM-SNSPD and 8M-PGM-SNSPD with 5×10^3, 5×10^4, 5×10^5 (only for PGM-SNSPD) stray photons per second, respectively. Figure 7 displays the performances of PGM-SNSPD and FM-SNSPD. However, the SDE for channel 1 of 500k-PGM-SNSPD can always be higher than that of FM-SNSPD. Meanwhile, the SDE for channel 2 of 500k-PGM-SNSPD would be smaller than that of FM-SNSPD in a region. We attribute this phenomenon to the difference in electrical characteristics. More significantly, the DCR of PGM-SNSPD can be suppressed to a low level without reducing the maximum SDE in either channel. Actually, as shown in Figs. 7(b) and 7(d) 500k-PGM-SNSPD can suppress the DCR more than three orders of magnitude than FM-SNSPD. The DCR of 8M-PGM-SNSPD can be decreased to 2% of FM-SNSPD.

Chen *et al.* pointed that the DCR with illumination is different from that without illumination and the calculation of the SDE may be inaccurate.[23] Therefore, we introduce the time-correlated single-photon counting (TCSPC) technique to analyze the temporal histogram for the 500k-PGM-SNSPD and the FM-SNSPD with 5×10^3, 5×10^4, 5×10^5 stray photons per second. Notably, the idle gate pulse, producing no effect on photons responses, will also be counted by TCSPC and we can distinguish it easily in the time region.

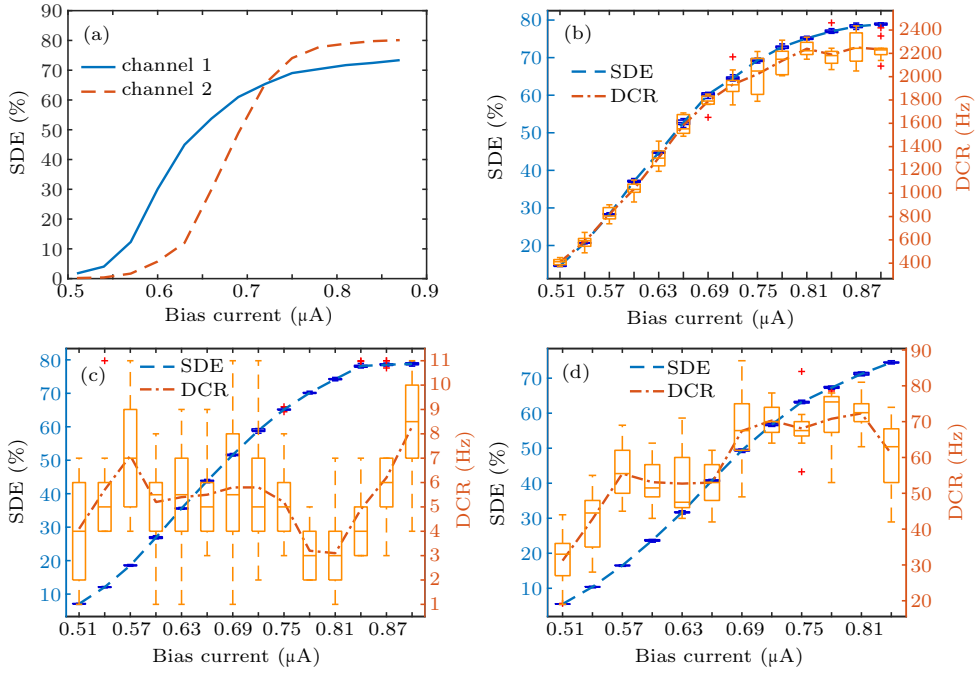


Fig. 6. (a) The system detection efficiency (SDE) for two channels of the PGM-SNSPD in which the blue line is result for channel 1 and the red line is for channel 2 of the PGM-SNSPD. These measurements are taken on about 8:00 of two days, with similar weather. (b) The SDE and dark count rate (DCR) of channel 1 of FM-SNSPD injected with stray photons to simulate 2000 DCR with maximum SDE. (c) The SDE and DCR of channel 1 of 500k-PGM-SNSPD injected with the same stray photons as (b). (d) The SDE and DCR of channel 1 of 8M-PGM-SNSPD injected with the same stray photons as (b). In all situations, we attenuate the pulse light of 500000 to 0.1 photon/pulse as the input of the SNSPD.

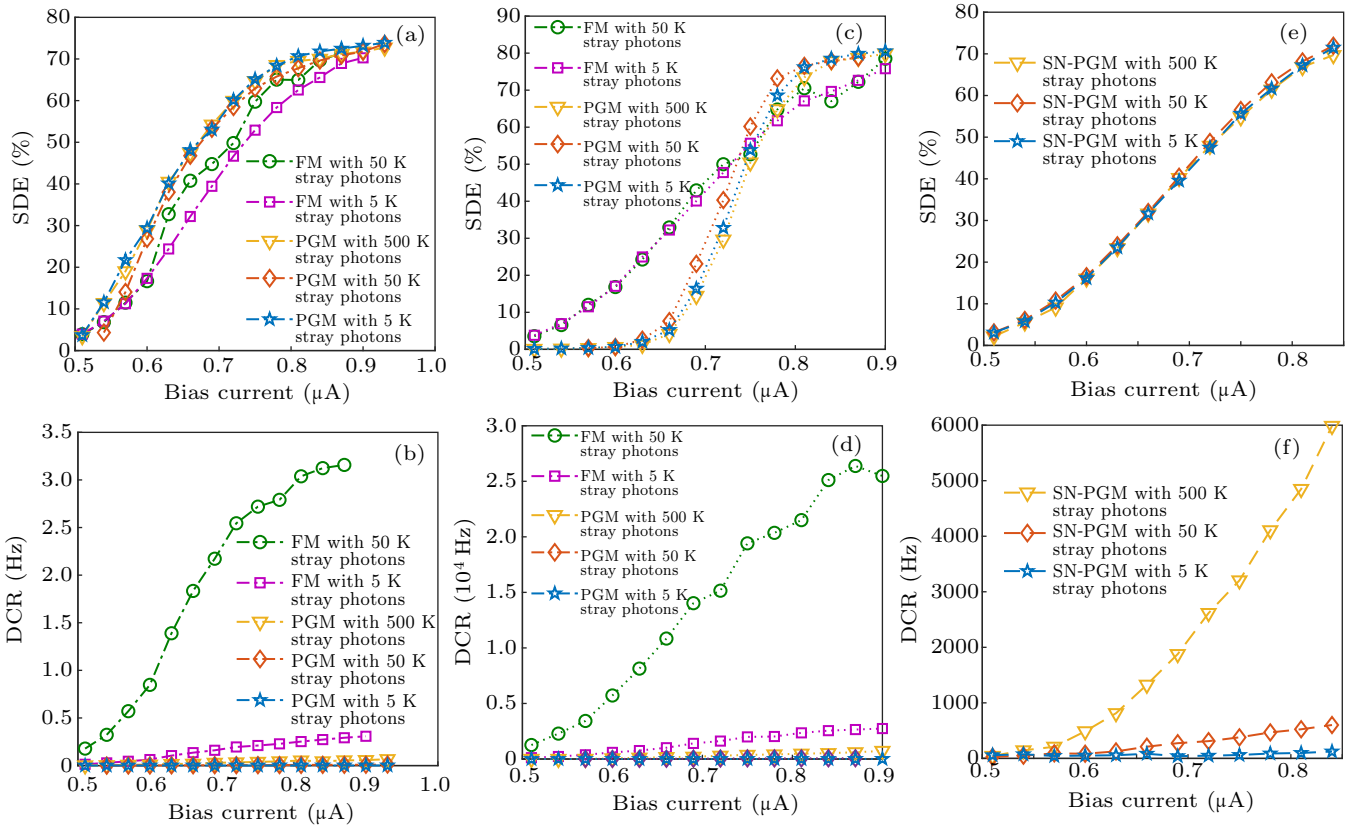


Fig. 7. The SDE and DCR for two channels of FM-SNSPD, 500k-PGM-SNSPD and, 8M-PGM-SNSPD (only for channel 1) with 5×10^3, 5×10^4, 5×10^5 photons per second (only for PGM-SNSPD). Here (a) and (c) are the SDE for two channels of 500k-PGM-SNSPD and FM-SNSPD. The former is the channel 1 and the latter is channel 2. The DCRs are displayed as the order of (a) and (c), in (b) and (d). Also, (e) and (f) present the SDE and DCR for channel 1 of 8M-PGM-SNSPD. These measure are taken in a dark room to avoid the influence of natural light and the stray photons are emulated by a 1550 nm continuous wave laser with flux of 5×10^3, 5×10^4, 5×10^5 photons per second.

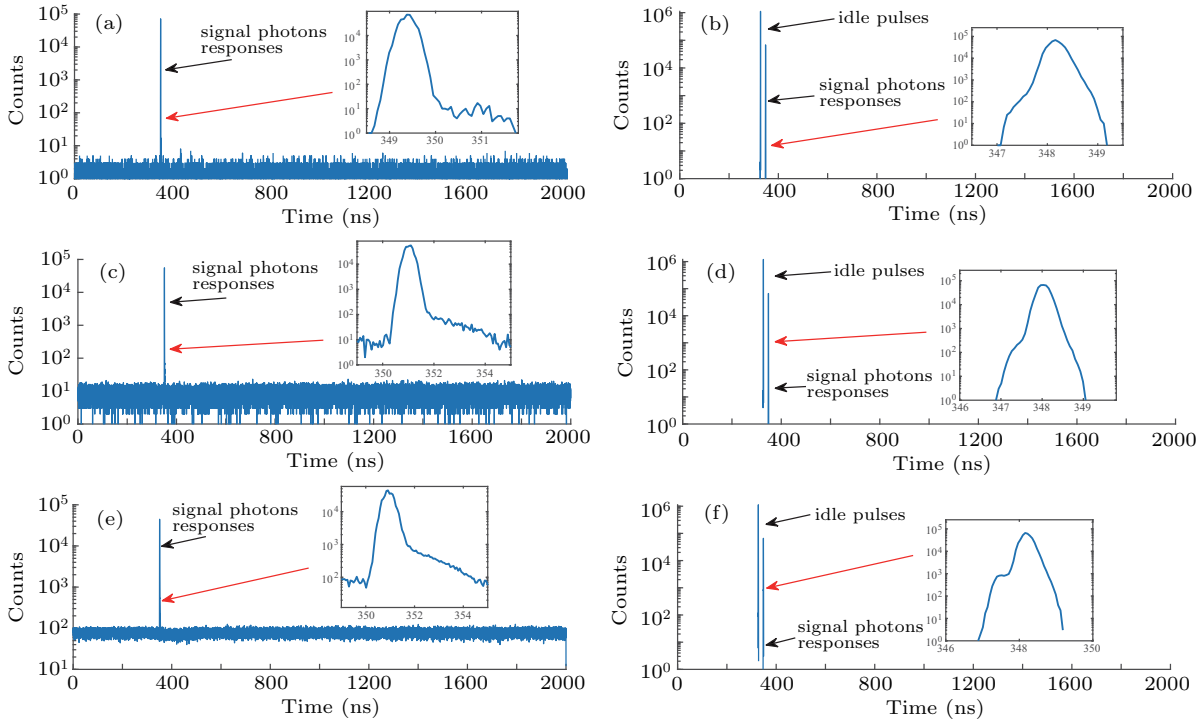


Fig. 8. Semi logarithmic temporal histograms for counts from FM-SNSPD, 500k-PGM-SNSPD with 5×10^3, 5×10^4, 5×10^5 stray photons per second in logarithmic coordinates. Here (a), (c), (e) are the results of FM-SNSPD with 5×10^3, 5×10^4, 5×10^5 stray photons per second, and (b), (d), (f) are the results of PGM-SNSPD with 5×10^3, 5×10^4, 5×10^5 stray photons per second. All the insets show greater details of the width of signals, which represent the time jitter of SNSPD. The stray photons were generated by a 1550 nm CW laser and coupled to the signal photons by a beam-splitter before the input of SNSPD. The time window is 2000 ns, and the window resolution is 64 ps, the collecting time is 10 s. Note that many data points in (a), (c) and (d) overlap owing to the resolution limit on displaying and printing.

Figure 8 shows that photons, only lacked at the peak of pulse gate, can be detected in the 500k-PGM-SNSPD, while signal responses can be every time slots in FM-SNSPD. As clearly evidenced from the results, the 500k-PGM-SNSPD effectively suppresses the signal response outside the pulse gate, while still maintaining a high SDE. Remarkably, the insets in Fig. 8 show the great detail of the signals. Since the TCSPC only measures the arrival time of signals, the width of the signal represent the time jitter of SNSPD. It is obvious that the time jitter of the 500k-PGM-SNSPD keeps pace with its main regions of the FM-SNSPD. In addition, there would be no smearing, which may be caused by stray photons.

Furthermore, we carried out a long-time measurement about 10000 s to obtain the accurate iDCR of 500k-PGM-SNSPD in a dark room and the final results indicate that the 500k-PGM-SNSPD can suppress the iDCR to 4.56×10^{-2} counts per second with SDE of 76.4372%.

6. Conclusions

As shown in simulations and experiments, PGM-SNSPDs obviously satisfy the requirements of most applications, which demand SNSPD with both high SDE and low DCR, especially in environments with numerous stray photons, e.g., in the free-space quantum key distribution and coexistence of quantum key distribution and data on optical fiber. In addition, the influence of Raman noise into the fiber can also be suppressed by PGM-SNSPDs, when adopting dense wavelength division multiplexing. However, due to the extraction method of signals, the interval between the two pulse gates cannot be less than the width of signals. In our experiments, we can only push the repetition frequency to 8 M, which may not be too high. Fortunately, there is much effort to reduce the recovery time of the SNSPDs, which helps to increase the repetition frequency.

In summary, SNSPDs can be operated in PGM at the same SDE as FM, but with fewer DCR. We have demonstrated the pulse-gated mode operation of commercial SNSPDs to suppress DCR to 4.56×10^{-2} counts per second with SDE of 76.4372%. Not only in a mild condition, but also on extreme test conditions, PGM-SNSPDs still have the superiority of suppressing DCR. To be specific, the 500k-PGM-SNSPD could suppress the DCR more than three orders of magnitude and 8M-PGM-SNSPDs can also decrease the DCR to 4%. Furthermore, the TCSPC analysis also approves the validity of our pulse-gated mode in suppressing response of stray photons. Indeed, the pulse-gated mode operation is also effective for the free-space optical coupled SNSPD, as ambient blackbody radiation and stray photons may be more serious than that in fiber-coupled SNSPDs. Although there is limitation of the repetition frequency of pulse gate, the work on reducing the recovery time of SNSPDs will improve it.

References

[1] Gol'tsman G N., Okunev O, Chulkova G, Lipatov A, Semenov A, Smirnov K, Voronov B, Dzardanov A, Williams C and Sobolewski R 2001 *Appl. Phys. Lett.* **79** 705

[2] Hadfield, Robert H 2009 *Nat. Photon.* **3** 696

[3] Natarajan C M, Tanner M G and Hadfield R H 2012 *Superconduct. Sci. Technol.* **25** 063001

[4] Eisaman M D, Fan J, Migdall A and Polyakov S V 2011 *Rev. Sci. Instrum.* **82** 071101

[5] Gemmell N R, McCarthy A, Liu B, Tanner M G, Dorenbos S D, Zwiller V, Patterson M S, Buller G S, Wilson B C and Hadfield R H 2013 *Opt. Express* **21** 5005

[6] Biswas A, Kovalik J, Srinivasan M, Shaw M, Piazzolla S, Wright M and Farr W 2016 *Proc. SPIE* **9739** 97390Q

[7] Takesue H, Nam S W, Zhang Q, Hadfield R H, Honjo T, Tamaki K and Yamamoto Y 2007 *Nat. Photon.* **1** 343

[8] Miki S, Yamashita T, Terai H and Wang Z 2013 *Opt. Express* **21** 10208

[9] Marsili F, Verma V B, Stern J A, Harrington S, Lita A E, Gerrits T, Vayshenker I, Baek B, Shaw M D, Mirin R P and Nam S W 2013 *Nat. Photon.* **7** 210

[10] Rosenberg D, Kerman A J, Molnar R J and Dauler E A 2013 *Opt. Express* **21** 1440

[11] Yang X, Li H, Zhang W, You L, Zhang L, Liu X, Wang Z, Peng W, Xie X and Jiang M 2014 *Opt. Express* **22** 16267

[12] Shibata H, Shimizu K, Takesue H and Tokura Y 2015 *Opt. Lett.* **40** 3428

[13] Shibata H, Shimizu K, Takesue H and Tokura Y 2013 *Appl. Phys. Express* **6** 072801

[14] Wang S, Chen W, Guo J F, Yin Z Q, Li H W, Zhou Z, Guo G C and Han Z F 2012 *Opt. Lett.* **37** 1008

[15] Yamashita T, Miki S, Makise K, Qiu W, Terai H, Fujiwara M, Sasaki M and Wang Z 2011 *Appl. Phys. Lett.* **99** 161105

[16] Bahgat Shehata A, Ruggeri A, Stellari F, Weger A, Song P, Sunter K, Najafi F, Berggren K and Anant V 2011 *Rev. Sci. Instrum.* **82** 071101

[17] Yamashita T, Miki S, Qiu W, Fujiwara M, Sasaki M and Wang Z 2010 *Appl. Phys. Express* **3** 102502

[18] Wu G, Zhou C, Chen X, Li X and Zeng H 2004 *Proc. SPIE* **5280** 812

[19] Akhlaghi M K and Majedi A H 2012 *Opt. Express* **20** 1608

[20] https://www.sconphoton.com/productinfo/1463565.html

[21] Kerman A J, Dauler E A, Keicher W E, Yang J K W, Berggren K K, Gol'tsman G and Voronov B 2006 *Appl. Phys. Lett.* **88** 111116

[22] Engel A, Semenov A, Hübers H W, Ilin K and Siegel M 2004 *Nucl. Instrum. Methods Phys. Res. Sect. A* **520** 32

[23] Chen S, You L, Zhang W, Yang X, Li H, Zhang L, Wang Z and Xie X 2015 *Opt. Express* **23** 10786